Engineering Geology 254 (2019) 76–88

Contents lists available at ScienceDirect

Engineering Geology

journal homepage: www.elsevier.com/locate/enggeo

Bayesian network models for probabilistic evaluation of earthquake-induced liquefaction based on CPT and V_s databases

Jilei Hu[a,b], Huabei Liu[b,*]

[a] School of Civil Engineering and Architecture, Wuhan Institute of Technology, Wuhan, Hubei 430074, China
[b] School of Civil Engineering and Mechanics, Huazhong University of Science and Technology, Wuhan, Hubei 430074, China

ARTICLE INFO

Keywords:
Bayesian network
Earthquake-induced liquefaction
Probabilistic prediction
In-situ tests

ABSTRACT

Cone penetration test (CPT) and shear wave velocity (V_s) based databases have been used for the evaluation of earthquake-induced soil liquefaction, but probabilistic evaluation of soil liquefaction using Bayesian network methods has seldom been attempted using CPT and V_s results. In this study, these databases are first used to construct two new Bayesian network (BN) models for predicting the probability of the occurrence of soil liquefaction and then compared with four simplified procedures and a Bayes classifier for soil liquefaction evaluation. The present study shows that the two new BN models are preferred over the simplified procedures and the Bayes classifier. The reasons for the better performance and advantages of the BN models are discussed. In addition, a converging BN model combing CPT, SPT (standard penetration test), and V_s databases is simultaneously attempted to further improve the prediction performance and applicability.

1. Introduction

Prediction procedures of earthquake-induced liquefaction based on in-situ tests (e.g., Seed and Idriss, 1971 and Seed and Idriss, 1982; Youd et al., 2001; Robertson and Wride, 1998; Moss et al., 2006; Idriss and Boulanger, 2006; Juang et al., 2009; Juang et al., 2012; Shen et al., 2016; Yang et al., 2017), such as the standard penetration test (SPT), cone penetration test (CPT), and shear wave velocity (V_s) techniques, have been extensively studied over the last several decades. These procedures are a function of the liquefaction resistance of soils in relation to the cyclic stress induced by seismic loadings. In these in situ tests, the SPT-based method for evaluating soil liquefaction is the most commonly used method throughout much of the world because it is widely available and inexpensive to perform (Youd et al., 2001). However, even though there are continued efforts to standardize the SPT procedures, there are still problems associated with its repeatability and reliability (Robertson et al., 1983); its discontinuity of data over depth easily results in missing the slightly thin soil layer (< 0.5 m), but potentially important liquefiable strata. Therefore, CPT is becoming increasingly popular as an in-situ test for site investigation and geotechnical design due to its simplicity, reproducibility, accuracy, and fully continuous profile, and it is more amenable to rational analysis (Robertson et al., 1983). However, the only limitation of the test is that it cannot directly identify soil types along the borehole. In addition, the SPT and CPT are large-strain tests that do not test the soil in an undisturbed state, but the V_s directly related to small-strain shear modulus is capable of avoiding the problem. V_s is similarly correlated to the cyclic resistance ratio (CRR) that is influenced by many variables that influence soil liquefaction, such as soil density, effective confining stresses, stress history, and geologic age (Youd et al., 2001). The procedure based on the V_s data for evaluating sandy and silty soil liquefaction was also applicable and very attractive due to its advantages. There exists a large body of well-known literature about developing CPT and V_s based procedures for predicting soil liquefaction as a classification problem using cyclic resistance ratio versus cyclic stress ratio (e.g., Robertson and Wride, 1998; Moss et al., 2006; Olsen and Koester, 1995; Idriss and Boulanger, 2008; Boulanger and Idriss, 2014; Andrus and Stokoe II, 1997; Andrus and Stokoe II, 2000).

Even though the aforementioned simplified methods have been proven to be reliable, most of them are generally known as deterministic approaches, in which case they did not consider the effect of the uncertainties associated with parameters and models. However, a probabilistic evaluation method is generally preferred in terms of the probability of liquefaction, and it can lead to a better engineering decision for anti-liquefaction treatment (Juang et al., 2006). The Bayesian framework method provides such a statistical probability technique, which allows for appropriate treatment of various contributing sources of aleatoric and epistemic uncertainty and allows for the simultaneous

* Corresponding author at: School of Civil Engineering and Mechanics, Huazhong University of Science and Technology, Wuhan, Hubei 430074, China.
E-mail address: hbliu@hust.edu.cn (H. Liu).

https://doi.org/10.1016/j.enggeo.2019.04.003
Received 5 December 2018; Received in revised form 31 March 2019; Accepted 2 April 2019
Available online 11 April 2019
0013-7952/

use of more descriptive variables as a high-order problem than most prior studies (Seed et al., 2003). This method also has the flexibility to fit any given mathematical form by accommodating its uncertainty associated with both the phenomena of soil liquefaction and the attempt to quantify the phenomenon (Moss et al., 2006). Cetin (2000) and Moss et al. (2006) have proven that the Bayesian updating method is useful for estimating the probability of soil liquefaction. Yazdi and Moss (2017) then proposed a Bayesian framework for the liquefaction triggering threshold combined with the kernel density estimation (KDE) method that provides a nonparametric likelihood function. For the Bayesian network (BN) method, it is a probabilistic graphical network based on the Bayesian theorem, which can quantitatively express the relationship between any two variables. The BN method plays an important role in risk probability analyses. Its key advantages are the integration of domain knowledge or prior knowledge and multisource information into a consistent system, and not only a forward inference (prediction) but also a backward analysis (diagnosis) (Tang et al., 2018). Due to its advantages, BN has been successfully applied in many fields. However, its applications in seismic liquefaction prediction based on in-situ tests data are relatively less (Bayraktarli, 2006; Bensi et al., 2011; Hu et al., 2015,2016; Hu and Liu, 2019).

However, the existing BN models can only be applied for predicting seismic liquefaction based on the SPT data. There still is not any BN model for predicting earthquake-induced liquefaction potential based on the CPT and V_s data. Therefore, one of the aims of this study is to construct two BN models for evaluating liquefaction potential based on each of the CPT and V_s databases. Four simplified models and a Bayes classifier based on CPT and V_s measurements are selected for comparison with the new BN models (the BN-CPT and BN-V_s models) in this study using 5-fold cross-validation. The selected simplified models are the Boulanger and Idriss method (Boulanger and Idriss, 2014) referred to as CPT-BI, the Moss model (Moss et al., 2006) referred to as CPT-MO, the Andrus and Stokoe model (Andrus and Stokoe II, 2000) referred to as V_s-AS, and the Kayen model (Kayen et al., 2013) referred to as V_s-KA (see Appendices). The selected Bayes classifier was proposed by Yazdi and Moss (2017) and is referred to as CPT-YM in the following presentation. In addition, another contribution of this study aims to converge the SPT, CPT and V_s databases into a system to further improve the performance of the BN model for evaluating seismic liquefaction.

2. Historical liquefaction datasets

2.1. Case selection

Liquefaction correlations are based on observation of the manifestations of liquefaction, e.g., ground cracking, sand boils, lateral spreading, tilting or settlement of buildings, and uplift of lifelines. Field case histories based on SPT, CPT, and V_s databases in this paper were collected from numerous earthquake events around the world that occurred from 1964 to 2011. Table 1 shows a summary of the range of values of part variables in the databases, of which $(N1)_{60cs}$ (Idriss and Boulanger, 2010) can be calculated by

$$(N1)_{60,CS} = (N1)_{60} + \exp\left[1.63 + \frac{9.7}{FC + 0.01} - \left(\frac{15.7}{FC + 0.01}\right)^2\right] \quad (1)$$

where $(N1)_{60,\ CS}$ is the corrected SPT blow count for the effective overburden stress and fines content, $(N1)_{60}$ is the normalized SPT blow count, and FC is the fines content. q_{c1Ncs} and V_{s1} are the corrected measured values that can be calculated by Eqs. (A8) and (C4) in the Appendices, respectively. In the three in-situ test databases, the SPT database consists of 308 cases that are obtained from Hu and Liu (2019). The CPT database consists of 410 cases (300 liquefaction cases and 110 non-liquefaction cases), and they are taken from Moss et al. (2006) and Boulanger and Idriss (2014). The V_s database consists of 465 cases, of which 330 cases are liquefied cases and the other 135 cases are non-liquefied cases, they are derived from Dong (2010), Cao (2010), Kayen et al. (2013), and Wood et al. (2017). Most of these cases have been reviewed, screened, and corrected by a panel of experts to result in robust databases (Moss et al., 2006; Boulanger and Idriss, 2014; Kayen et al., 2013; Wood et al., 2017), such as separating liquefied soils from clays, corrections to the influence of vertical effective stress, fines content, and the duration of the ground motion, and generating an individual case in a single site. The rest of the cases from China have also been processed according to the criterion.

However, to obtain higher quality liquefaction cases for constructing the assessment model, further data processing is of prime importance in this study to minimize epistemic uncertainty as follows: (1) any individual case can produce only one performance outcome, such as either liquefaction or non-liquefaction. Therefore, all marginal liquefaction cases should be eliminated in this study. (2) Since soil-structure interaction might have significantly influenced soil liquefaction, sites adjacent to the structures within 10 m are not considered in the dataset. (3) Except for fines content, if other factors of soil liquefaction, e.g. groundwater table or vertical effective stress, etc., are missing values, cases with the situation will be eliminated. (4) If liquefied or non-liquefied fields without the acceleration time history, the cases will be eliminated, because the root mean square of acceleration a_{rms} instead of peak ground acceleration (PGA) is used in this study to construct the BN models. Since a_{rms} that includes the information of the amplitude, frequency content, and duration of the strong motion can reflect the energy of random ground motion to some extent, whereas PGA only reflects the amplitude of the earthquake motion, a_{rms} is more suitable to evaluate seismic liquefaction than PGA (Hu and Liu, 2019). Most of the acceleration records adjacent to the cases were downloaded from the websites http://www.strongmotioncenter.org/ and https://ngawest2.berkeley.edu/, and other acceleration records from some Chinese earthquakes were provided by the China Strong Motion Network Centre at the Institute of Engineering Mechanics, China Earthquake Administration. All of the acceleration records are used to calculate the root-mean-square acceleration a_{rms} by

$$a_{rms} = \sqrt{\frac{1}{t_d}\left(\int_{t_5}^{t_{95}} a_x^2(t)dt + \int_{t_5}^{t_{95}} a_y^2(t)dt\right)} \quad (2)$$

where a_x is the horizontal ground acceleration in the x-direction; a_y is the one in the y-direction; t_5 and t_{95} are the moments at 5% and 95% of Arias intensity, respectively; t_d is the relative duration, where $t_d = t_{95} - t_5$.

2.2. Critical layer selection

Selection of the critical layer is always difficult, but it is also an important step in predicting earthquake-induced liquefaction. The critical layer is the most eminently liquefiable stratum of soil that constitutes the weakest link in the chain from a liquefaction perspective (Moss et al., 2006). In this study, its identification criteria are as follows: (1) the critical layer must be deposited below the groundwater table. (2) The clay layer is considered a non-liquefiable soil that should be eliminated from the candidates for the critical layer. It can be identified by SPT borehole data or by using some simple methods (e.g., Ching et al., 2015; Cao et al., 2018; Wang et al., 2018; Wang et al., 2019). (3) The candidates should contain stable measured values. (4) The stratum with the least measured value or the smallest CRR in the profile is defined as the critical layer. A thorough discussion of the selection of the critical layer and related issues can be found in Moss et al. (2006) and Wood et al. (2017).

For the sites that have SPT, CPT, V_s profiles simultaneously, in addition to the aforementioned four criteria, another two criteria were considered in this study as follows: (1) the distance between each CPT and SPT pair or each V_s and SPT pair should be < 30 m to be treated as

Table 1
Ranges of values for part variables of case histories in the SPT, CPT, and V_s databases.

Earthquake	M_w	a_{rms} (m/s^2)	Depth (m)	GWT (m)	SPT cases		CPT cases		V_s cases	
					$(N1)_{60cs}$	No.	q_{c1Ncs}	No.	V_{s1} (m/s)	No.
1964 Niigata	7.6	0.33	3.1–11.2	0.5–2.0	7.8–30.6	5	26–184	9	120–188	5
1968 Tokachi-Oki	8.3	0.50–0.58	4.0–6.0	0.9–1.0	11.0–11.5	2	–	0	139–148	2
1978 Miyagiken-Oki	7.7	0.10	3.3–6.0	0.9–3.0	8.0–13.7	4	–	0	141–165	4
1979 Imperial Valley	6.5	0.24–2.42	1.8–6.5	1.2–2.7	8.5–40.9	20	33–254	21	109–339	12
1980 Mexicali	6.3	1.40	2.3–3.0	2.0–2.2	–	0	54–96	4	–	0
1981 Westmorland	6.9	0.55–1.72	2.4–4.8	1.2–2.7	7.5–20.4	9	58–145	12	102–194	9
1983 Nihonkai-Chubu	7.7	0.41–0.59	1.8–5.7	0.4–1.0	10.1–13.9	2	35–37	2	123–139	2
1987 Superstition Hills	6.2	0.43	4.6	1.2	27.0	1	113	1	190	1
1987 Superstition Hills	6.5	0.44–0.57	2.4–3.9	1.2–2.7	8.5–21.7	4	76–159	4	120–212	5
1989 Loma Prieta	6.9	0.32–1.24	1.5–8.5	0.8–6.4	3.5–43.2	100	14–254	132	100–249	94
1993 Kushiro-Oki	7.6	0.76–1.24	2.5–8.0	1.0–2.0	13.6–20.7	2	–	0	119–198	8
1993 Hokkaido-Nansei	8.3	0.43–0.67	1.5–7.5	0.9–2.0	–	0	–	0	124–210	6
1994 Northridge	6.7	1.13–2.90	3.9–9.8	3.3–7.2	10.2–17.1	3	91–131	3	143–171	4
1995 Hyogoken-Nambu	6.9	1.31–3.15	3.3–18.5	1.4–4.4	5.0–12.3	2	16–184	15	174–179	31
1999 Kocaeli	7.4	0.83–0.99	1.0–10.0	0.4–3.3	5.7–34.9	6	16–131	18	53–261	43
1999 Chi-Chi	7.6	0.52–1.71	1.0–16.5	0.4–4.0	7.2–27.8	5	34–197	58	52–261	32
2000 Geiyo-Hiroshima	6.8	0.59	2.5–10.5	1.0–3.0	–	0	–	0	158–179	3
2000 Torrori-Seibu	6.8	0.85	5.6–6.0	1.0–2.0	–	0	–	0	100–130	3
2002 Denali Fault	7.9	0.81	1.8–2.4	0.5–1.0	–	0	–	0	149–173	2
2003 Tokachi-Oki	7.8	1.09	2.6–9.0	1.0–2.0	–	0	–	0	125–164	7
2003 Bachu	6.8	0.08–0.16	2.4–13.9	0.4–4.2	7.2–46.4	38	25–203	38	145–249	55
2008 Wenchuan	7.9	0.19–1.71	2–11.9	0.8–8.1	2.4–44.0	45	–	0	154–474	45
2010 Darfield	7.1	0.52–1.00	1.7–8.6	0.5–2.4	3.5–33.1	25	35–146	25	115–202	25
2011 Christchurch	6.2	0.77–2.56	1.7–9.5	0.5–3.3	2.8–34.2	65	35–206	65	98–221	65
2011 Tohoku	9.0	0.41	4.8–9.0	1.1–1.3	–	0	98–132	3	139–140	2
Gross	6.2–9.0	0.08–3.15	1.0–18.5	0.4–8.1	2.4–46.4	308	14–254	410	52–474	465

Note: M_w is the earthquake magnitude, and GWT is the groundwater table.

the same soil profile (Akca, 2003); and (2) the critical layer with the least measured values of SPT, CPT, V_s should be in the same soil layer. After employing these six criteria, 210 cases were identified to have relevant SPT, CPT, V_s profiles simultaneously. The average measurement of a critical layer in each case is calculated to characterize the liquefaction resistance of the layer. In addition, if a non-liquefaction profile is observed, the stratum with the largest measured value of SPT, CPT, or V_s is defined as a non-liquefied layer (Ku et al., 2004; Dong, 2010).

2.3. Experimental design

The BN method can show sufficient prediction accuracy even with rather small sample sizes (Kontkanen et al., 1997). It is therefore believed that the sample sizes of the CPT and V_s datasets in this study are adequate. This study divided the databases into a training set and a validation set. The CPT and V_s databases are randomly divided into 5 folds; the ratios of liquefaction samples to non-liquefaction samples were fixed at approximately 2.7:1 (60 liquefaction samples and 22 non-liquefaction samples) and 2.4:1 (66 liquefaction samples and 27 non-liquefaction samples) in each of the fold data sets. In the crossover trial, four folds were used to train the BN models, and the remaining single fold was utilized to validate performances of the BN models. The above process was repeated 5 times so that all of the samples can be used for either training or validating.

3. Constructing new BN models

3.1. A brief description of a BN

A Bayesian network is a combination of probability theory and graph theory, and it is a powerful tool for expressing and inferring uncertain knowledge including parameter and model uncertainties based on the Bayes theorem (Pearl, 1988). A BN model $B(G,P)$, wherein G is a directed acyclic graph that contains various nodes and links, and these nodes are random variables that are connected with links expressing causal relations or probabilistic relations; P is the conditional probability table of each node that can quantify the relationship between two nodes. Thus, the posterior probability of any variable in the model can be calculated by the Bayesian formulas and conditional independence rule as follows:

$$P(X_i \mid Y) = \frac{P(Y \mid X_i)\cdot P(X_i)}{P(Y)} \tag{3}$$

$$P(Y \mid x_1, x_2, \cdots, x_n) = \frac{P(x_1, x_2, \cdots, x_n \mid Y)\cdot P(Y)}{P(x_1, x_2, \cdots, x_n)} = \frac{P(x_1, x_2, \cdots, x_n \mid Y)\cdot P(Y)}{P(x_1)P(x_2 \mid x_1)\cdots P(x_n \mid x_1, x_2, \cdots, x_{n-1})} \tag{4}$$

$$P(x_1, x_2, \cdots, x_n) = \prod_{i=1}^{n} P(x_i \mid \pi(x_i)) \tag{5}$$

where $x_1, x_2, \cdots, x_n$ and Y are random variables; $P(X_i \mid Y)$ is the posterior probability of variable X_i given evidence Y, which incorporates both the subjective and objective information into the distributions of the model variables; $P(X_i)$ and $P(Y)$ are the prior probabilities of variable X_i and Y and include subjective information about the distributions of the variables; $P(Y \mid X_i)$ is the likelihood that the statistical measurements are associated with the objective information and is proportional to the conditional probability of observing a particular event given evidence X_i; $P(x_1, x_2, \cdots, x_n)$ is the joint probability of variables $x_1, x_2, \cdots, x_n$; and $\pi(x_i)$ is a set of values for the parents of X_i. Eq. (3) represents backward inferring, and Eq. (4) represents forward reasoning.

In liquefaction prediction, enormous amounts of historical information about earthquake-induced liquefaction are accumulated, such as the liquefaction manifestation, the relationship between influence variables of liquefaction, and standard specification, which can be served as effective prior knowledge for determining the structure of a BN model for predicting liquefaction. Therefore, prior knowledge is used for constructing the structure of BN models for avoiding unreasonable relationships caused by overfitting, and data learning is utilized for obtaining the conditional probability tables of nodes in the

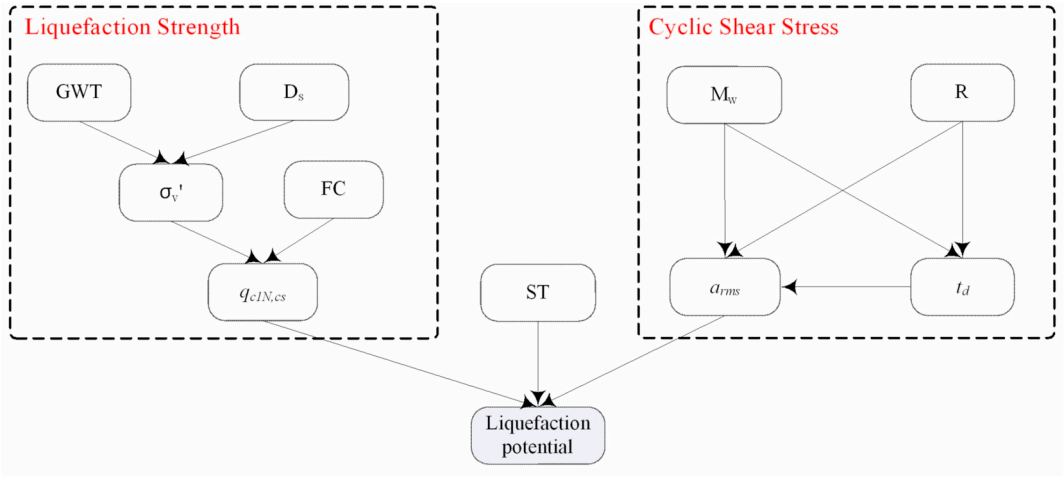

(a) A BN-CPT model

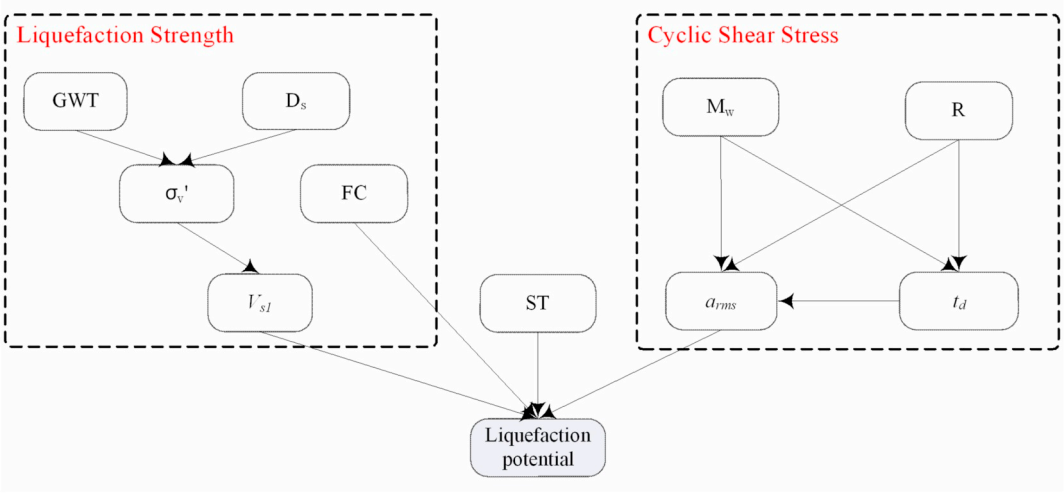

(b) A BN-V_s model

Fig. 1. Two new BN models for evaluating soil liquefaction based on the CPT and V_s tests.

structure. This study used two algorithms, gradient descent algorithm (Jensen, 1999) and expectation maximization (Lauritzen, 1995), for parameter learning under the condition of complete data and incomplete data, respectively. Hu et al. (2017) proved that the performances of these two algorithms applied in liquefaction prediction are slightly different.

3.2. Building structures of BN models

Hu and Liu (2019) constructed two BN models using the earthquake magnitude (M_w), epicentral distance (R), root-mean-square acceleration (a_{rms}) or peak ground acceleration (PGA), relative duration (t_d), soil type (ST), groundwater table (GWT), depth of soil deposit (D_s), fines content (FC), vertical effective stress (σ_v'), and corrected SPT blow count for the effective overburden stress and fines content ($(N1)_{60cs}$) combing extensive knowledge or mechanism of earthquake-induced liquefaction and a large amount of historical SPT data, and they proved that the BN-a_{rms} model performed better than the BN-PGA model.

Therefore, $(N1)_{60cs}$ is replaced by q_{c1Ncs} and V_{s1} based on the BN-a_{rms} model to construct the other two new BN models in this study (shown in Fig. 1), and links between other variables in the BN-a_{rms} model are kept. However, a small difference in the BN-V_s model is that the fines content does not have a link with V_{s1} due to their lack of a strong relationship (Kayen et al., 2013), but the fines content is related to the liquefaction potential with a link between them (Thevanayagam, 1998). The structures of the two new BN models take into account the physical relations and conditional independence between all variables, which can eliminate redundant links and make the modelling interpretable. In addition, the BN models regard the evaluation of earthquake-induced liquefaction as a high-dimensional classification problem that allows them to contain all the data information.

3.3. Parameter learning

After completing the structures of the above BN models, parameter learning needs to be processed to obtain the conditional probability tables of variables in the BN models. Due to lack of values for defining the fines contents and soil types in the V_s database, an expectation maximization algorithm was used to complete parameter learning, whereas a gradient descent algorithm was adopted for parameter learning in the CPT database. Although there was a lack of values for the fines contents and soil types, the values can be estimated by the soil behavior type index, I_c, proposed by Robertson and Wride (1998), Ching et al. (2015) and Cao et al. (2018).

In the processing of parameter learning, the continuous variables in the models should be discretized because the distribution functions of the continuous variables are not required (Friedman and Goldszmidt, 1996). Except for FC, q_{c1Ncs}, and V_{s1}, the grading standards of the remaining variables can be found by referring to Hu et al. (2016) and Hu and Liu (2019). Hu et al. (2016) divided FC into three grades, < 30%, 30–50%, and > 50%, by using the equal frequent method, and they found that when FC is > 50%, the soils are not liquefied in their collected dataset. However, in the data sets of this paper, many soil types exist (e.g., silty soils) with an FC between 50% and 75% and were liquefied during the Chi-Chi earthquake in Taiwan and Kocaeli earthquake in Turkey. In addition, sandy soils with FC < 5% are considered to be clean sands (Youd et al., 2001), and the threshold of FC within approximately 35% takes over the matrix and controls the mechanical behavior (Thevanayagam, 1998). Therefore, the new grades of FC in this study are separated into those involving ≤5%, 5–35%, 35–75%, and ≥ 75% by domain knowledge. The limitations of V_{s1} of 210 m/s and q_{c1Ncs} of 160 are considered equivalent to a corrected blow count of 30 in sandy soils (Andrus and Stokoe II, 2000), and their remaining grades can be calculated by the formulas suggested by Andrus and Stokoe II (2000) and Idriss and Boulanger (2008), according to the grades of $(N1)_{60}$, which are ≤160 m/s, 160–175 m/s, 175–210 m/s for V_{s1}, and ≤ 80, 80–110, and 110–160 for q_{c1Ncs}.

3.4. Measurement index

To assess the performance of a model for predicting liquefaction potential, six common measurement indexes, the *Accuracy*, *Precision*, *Recall*, F_1 score, area under the curve of the receiver operating characteristic (*AUC* of ROC), and *Brier* score, are used in this study. *Accuracy* is the proportion of a number of correctly predicted samples to the total number of samples. In a classification task, *Precision* is also known as positive predictive value as it is the number of true positives (e.g., liquefaction is predicted and was observed) divided by the total number of instances predicted as the positive class (e.g., the sum of liquefaction and non-liquefaction samples, which are all predicted as liquefied instances). *Recall* in this context is also called sensitivity and is the proportion of the number of true positives to the total number of positive classes. Normally, a classifier has high *Precision* but lower *Recall*; thus, a compromised index, F_1 score, is the harmonic mean of the two indexes.

Receiver operating characteristic (ROC) analyses have been widely adopted to evaluate the performance of a classification model, which is gradually used in geotechnical engineering (e.g., Oommen et al., 2010; Maurer et al., 2015; Hu et al., 2016 and 2017; Hu and Liu, 2019). The ROC curve is a plot of TPR (True Positive Rate) versus FPR (False Positive Rate) at various threshold settings, as shown in Fig. 2. TPR is also known as sensitivity or *Recall*. FPR is also known as the probability of false alarm and can be calculated as 1-specificity (e.g., liquefaction is predicted, but did not occur). A perfect model plots along the left vertical and upper horizontal axes, connecting at point (0, 1). In ROC curve space, there exists an optimum threshold (e.g., the red dot in Fig. 2) for the model to perfectly segregate the dataset, and it can be determined on a point closest to the point (0, 1) or a cut-off threshold that maximizes the value of FPR + 1-FPR. The area under a ROC curve (AUC) is the area between the x-axis and the ROC curve, which ranges from 0.5 to 1. As such, a greater AUC indicates a better model performance.

In addition, the *Brier score,* proposed by Brier (1950), is a proper score function that evaluates the accuracy of probabilistic predictions or model bias for a classifier. The most common expression of the *Brier score* is

$$B = \frac{1}{n}\sum_{i=1}^{n}(f_i - E_i)^2 \quad (6)$$

where n is the total number of forecasting samples, f_i is the prediction probability, and E_i is the actual outcome of the event at sample i (e.g., 1 for liquefaction and 0 for non-liquefaction). The *Brier score* ranges from 0 to 1 for the binary classification, where $B = 0$ shows a perfect prediction and $B = 1$ denotes the worst possible prediction, i.e., the lower the Brier score is, the better the predictions are calibrated.

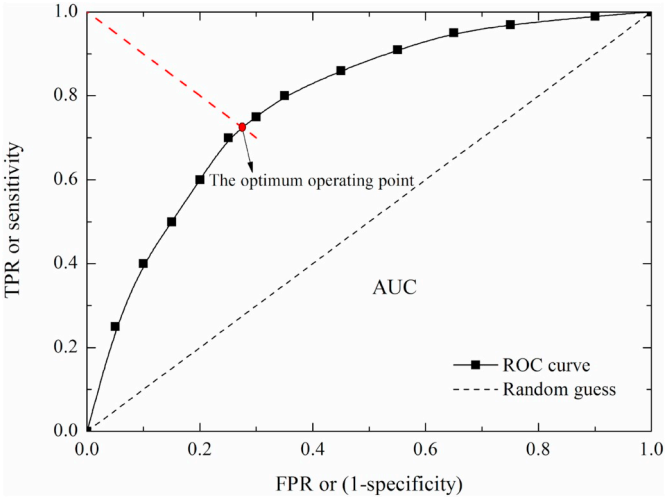

Fig. 2. ROC curve and the optimum operating point.

Each aforementioned measurement index will be calculated 5 times in 5-fold cross-validation, and their average, known as the macro mean, is employed to evaluate the performance of the BN models.

4. Results

4.1. Training performances of the BN models

Since the *accuracy*, *AUC* and F_1 can intuitively and comprehensively reflect the classification performance of a model, these three indexes are used to evaluate the learning ability of the two BN models. With the BN-CPT model, *Macro-Accuracy* = 0.885, *Macro-AUC* = 0.931, and *Macro-*F_1 = 0.923 for the liquefaction samples, which are all high, except that *Macro-*F_1 = 0.767 for the non-liquefaction samples, which is slightly low. In addition, With the BN-V_s models, *Macro-Accuracy* = 0.917, *Macro-AUC* = 0.974, and *Macro-*F_1 = 0.942 and 0.855 for liquefaction and non-liquefaction samples, respectively, are all very prominent. Therefore, these high values show that the two BN models have a good learning ability.

4.2. Comparison with existing models for the CPT data set

This section compares the new BN model based on CPT data with the CPT-BI model (Boulanger and Idriss, 2014), CPT-MO model (Moss et al., 2006), and CPT-YM model (Yazdi and Moss, 2017). Since the CPT-BI and CPT-MO models do not need to train models, only the comparison of predicting results of the four models is shown in Table 2. It can be seen that the BN-CPT model has the highest *Macro-Accuracy* and *Macro-*F_1*s* values for both non-liquefaction and liquefaction samples, which performs better than the CPT-BI, CPT-MO and CPT-YM models, while its *Macro-AUC* is the second highest that is slightly lower than that of the CPT-YM model. However, the *AUC* is not sensitive to sampling bias within the dataset, whereas the F_1 score is (Hu et al., 2015 and 2017). Hence, the F_1 is more suitable than the *AUC* to assess the performance of a model under the condition of sampling bias. Therefore, after comprehensively comparing the *accuracy* and F_1 scores, the general performance of the BN-CPT model for predicting soil liquefaction is preferable to those of the others, while the CPT-YM model has the second best performance. It should be noted that both the BN-CPT and CPT-YM models can be considered as Bayes classifiers, the

Table 2
Comparison of predicting results of CPT-based models.

Model	*Macro-accuracy*	*Macro-AUC*	Liquefaction			Non-liquefaction		
			Macro-recall	*Macro-precision*	*Macro-F_1*	*Macro-recall*	*Macro-precision*	*Macro-F_1*
BN-CPT	0.871	0.887	0.937	0.893	0.913	0.691	0.815	0.742
CPT-BI	0.839	0.863	0.890	0.890	0.890	0.700	0.699	0.699
CPT-MO	0.822	0.880	0.840	0.911	0.873	0.773	0.641	0.699
CPT-YM	0.866	0.891	0.953	0.875	0.912	0.627	0.833	0.715

Table 3
Comparison of predicting results of V_s-based models.

Model	*Macro-accuracy*	*Macro-AUC*	Liquefaction			Non-liquefaction		
			Macro-recall	*Macro-precision*	*Macro-F_1*	*Macro-recall*	*Macro-precision*	*Macro-F_1*
BN-V_s	0.880	0.903	0.930	*0.904*	0.916	0.756	0.823	0.784
V_s-AS	0.865	0.916	0.864	*0.941*	0.900	0.867	0.722	0.788
V_s-KA	0.867	0.922	0.882	*0.927*	0.904	0.830	0.742	0.783

differences between which lie in the dimensions for liquefaction classification and the parameter estimation methods.

4.3. Comparison with existing models for the V_s data set

A comparison of predicting results of V_s-based models in this study is shown in Table 3. It can be seen that the *Macro-Accuracy* of the BN-V_s model is higher than those of the V_s-AS and V_s-KA models. For different classes, the *Macro-F_1* score of the BN-V_s model for liquefaction class are higher than those of other models, and the *Macro-F_1* score for the non-liquefaction class of the three models are close to each other. Relatively small *Macro-AUC* of the BN-V_s model may be due to sampling bias (approximately 2.4:1 for liquefaction samples and non-liquefaction samples), while the *AUC* is not a reliable basis for evaluating model performance under the condition of sampling bias. Therefore, after comprehensively comparing *accuracy* and *F_1* scores, the BN-V_s model is slightly better than the other two models.

4.4. Sensitivity analysis and diagnosis in the two new BN models

Sensitivity analysis and diagnosis are described in this section to illustrate the performance of each input variable in terms of soil liquefaction, which can be used to obtain the posterior probability distribution of each variable for providing reliable scientific diagnosis when liquefaction occurs. The results of the sensitivity analysis of the two BN models are shown in Fig. 3. It can be clearly seen that q_{c1Ncs} and V_{s1}, with sensitivity indexes of 17.3% and 28.1%, respectively, are vital to the liquefaction potential in the corresponding BN models, and sensitivity indexes of a_{rms} and relative duration are the second and third maximum in both BN models. In addition, the relative sensitivities of *FC*, *ST*, *R*, σ_v', D_s, M_w, and *GWT* decreases in order in the BN-CPT model, whereas the relative sensitivities of σ_v', *R*, D_s, *GWT*, *ST*, M_w, and *FC* decrease in order in the BN-V_s model. The differences between the contributions of factors between the two BN models are caused by different in-situ testing data and slightly different structure.

Except for the accurate prediction of the BN models, they can also do backward inferences to simulate the evolution route of liquefaction occurrence in a short time. Fig. 4 shows the process of backward reasoning by using the 2011 Christchurch, New Zealand, earthquake as an example in the BN-CPT model. The status of M_w and *R* are defined as strong and medium, respectively. What kind of soil and field conditions easily result in liquefaction? First, the posterior probability distribution of the remaining input factors could be calculated by Eq. (3). The results, as seen in Fig. 4(a), indicate that a_{rms} = super with a 66.3% chance, t_d = medium with a 76.3% chance, *ST* = poor sand with a

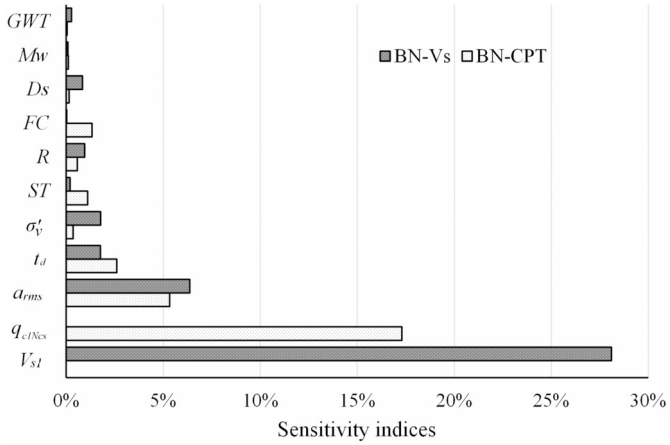

Fig. 3. Sensitivity indexes of 11 input variables in the BN-CPT and BN-V_s models.

60.9% chance, D_s = shallow with a 65.5% chance, and *FC* = medium with a 63.7% chance, are most likely to happen. Then, the status of the previously mentioned five factors could be entered into the BN model as extra evidence for the subsequent backward inference. The results, as seen in Fig. 4(b), illustrate that q_{c1Ncs} = loose with a 66.4% chance is more likely to occur. Finally, the status of q_{c1Ncs} is fixed as loose, and so forth, until all statuses of the remaining factors could be identified, as shown in Fig. 4(c)). σ_v' and *GWT* are small and shallow, with 60.3% and 53.0% chances, respectively. In general, the liquefaction diagnosis route of this example could be extracted, which may be a_{rms} = super, t_d = medium, *ST* = poor sand, and *FC* = medium → q_{c1Ncs} = loose →σ_v' = small, and *GWT* = shallow. All statuses of the factors in the diagnosis match some data (e.g., CPT-277 in Burwood during the 2011 Christchurch earthquake, New Zealand).

5. Discussion

5.1. Performances of a converging BN model

Since there might exist a paradox prediction result in the BN- SPT, CPT, and V_s models for the same case (Schneider and Moss, 2011), it is advisable to combine the BN models into a system for avoiding this problem. The converging BN model is constructed as shown in Fig. 5 by combining BN-SPT, BN-CPT, and BN-V_s models into a system. In this BN model, it can predict liquefaction potential based not only on one of the

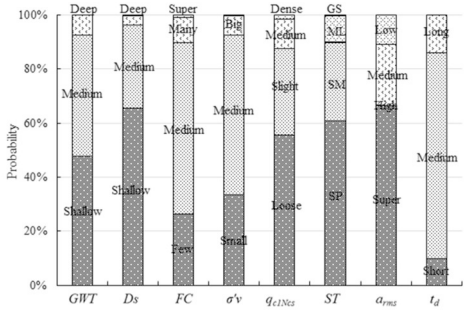

(a) P(*GWT*, *Ds*, *FC*, σ_v', q_{c1Ncs}, *ST*, a_{rms}, t_d | *LP* =Yes)

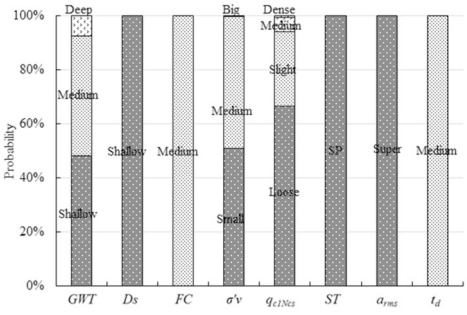

(b) P(*GWT*, σ_v', q_{c1Ncs} | *LP*= Yes, *Ds*= Shallow, *FC*= Medium, *ST*= SP, a_{rms}= Super, t_d= Medium)

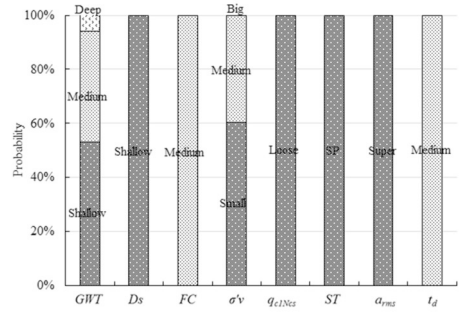

(c) P(*GWT*, σ_v' | *LP*= Yes, *Ds*= Shallow, *FC*= Medium, *ST*= SP, a_{rms}= Super, t_d= Medium, q_{c1Ncs}= Loose)

Fig. 4. The process of diagnosis of soil liquefaction suffered a strong earthquake in the BN-CPT model.

in-situ tests but also on multiple in situ tests. For example, when the model predicts liquefaction potential 1 based on SPT data, q_{c1Ncs}, V_{s1}, liquefaction potential 2, liquefaction potential 3, and liquefaction potential are taken as an unknown that has no effect on liquefaction potential 1 due to their conditional independence. However, when the model predicts liquefaction potential based on multiple in-situ tests, liquefaction potential 1, liquefaction potential 2, and liquefaction potential 3 are taken as unknowns to calculate the posterior probability of the liquefaction potential. In this study, there are only 210 sites (155 liquefaction cases and 55 non-liquefaction cases); these cases are fixed at approximately 2.8:1 to complete the 5-fold crossover trials. The results of the converging BN model for training and validating data are shown in Table 4. High values of *Macro-* indexes show that the BN model has good performance.

5.2. Comparison of four BN models

To compare the classification capacities of the four BN models, the 210 cases used in section 6 were used to train and validate the models. There are 148 cases for training and 42 cases for validating. Only two measures, *Macro-Accuracy* and *Macro-Recall* were used herein to detect their prediction accuracies. The results (see Fig. 6) show that the BN-converging model is better than the other three BN models in both training and validating data, whereas the BN-V_s model yields the worst *Macro-Accuracy* and *Macro-Recall* in the prediction. In addition, the BN-converging model can also predict the liquefaction potential of a site with one of the SPT, CPT, and V_s data by calculating posterior probabilities of liquefaction potential 1, liquefaction potential 2, or liquefaction potential 3. The *Macro-Accuracy* values of the BN-converging model in the validating data are 87.6% for the SPT data, 87.1% for the CPT data, and 84.8% for the V_s data, which are slightly greater than those of the corresponding BN models shown in Fig. 6. This is because liquefaction potentials 1, 2, and 3 are marginally independent with a link of a child note (Liquefaction potential) that slightly affects the posterior probabilities.

To further compare the model bias of the four BN models, average *Brier scores* of the BN- SPT, CPT, V_s and converging models in the 5 K-fold cross-validation are 0.098, 0.106, 0.110, and 0.079, respectively. It is obvious that the *Brier scores* of the four models are all relatively low, which shows that the four models have a small model bias, i.e., they have high probability predicting accuracy. In these four models, the model bias of the BN-Converging model is the smallest, the BN-SPT model is the second smallest, and the BN-V_s model performs the worst. This difference might be because the V_s value is directly related to the small-strain shear modulus, and it can be variable over short distances even within a single geologic unit (Thompson et al., 2007), whereas the liquefaction resistance of soils has a large-strain behavior (Seed et al., 2003). In addition, V_s-based methods are often dependent on supporting data obtained from either SPT or CPT tests such as soil type, groundwater table, and fines content. Thus, V_s-based methods should ideally not be performed alone (Green Russell et al., 2017). All in all, adopting a combination of several BN models can not only improve classification accuracy but also reduce model bias, even though relatively few data were collected in this study. Additionally, the BN method can perform well under the condition of the small sample size (normally, < 50 cases) problem by using the bootstrap approach to extend data (Friedman et al., 1999). Therefore, the performance of the BN-Converging model would improve if more data could be obtained in the future.

In process of prediction in the converging BN models, there existed several paradox prediction results, and examples with two liquefied sites and two non-liquefied sites are shown in Fig. 7. The optimum thresholds of the BN-SPT, BN-CPT, BN-V_s, and BN-converging models in this study are 0.6, 0.4, 0.5 and 0.5, respectively. Therefore, the predictions of the BN-SPT and BN-CPT models are wrong for sample 1; the BN-V_s model prediction is wrong for sample 2; all BN models prediction is wrong for sample 3; and the BN-CPT and BN-V_s predictions are wrong for sample 4. These results illustrate that the converging BN model would have better classification accuracy if one or two of the BN models for a single in-situ test data predicted correctly. However, if the three different BN models simultaneously predicted incorrectly, the prediction of the BN-Converging model cannot be correct. In addition, from the perspective of a single sample, the prediction probability accuracy of the BN-Converging model might be not the highest or lowest one, but its overall probability of prediction accuracy (i.e., *Brier score*) is the best. The reason that the BN-Converging is a better model than the BN models for the single in-situ test is that the posterior probability of liquefaction occurrence in the BN models for the single in-situ test is the probability of liquefaction potential providing evidence of its related variables. For instance, in the BN-SPT model, the posterior probability is P(LP = 1|$(N1)_{60cs}$, soil type, a_{rms}) for predicting soil liquefaction given values of $(N1)_{60cs}$, soil type, and a_{rms}, whereas the posterior probability in the BN-Converging model is changed into:

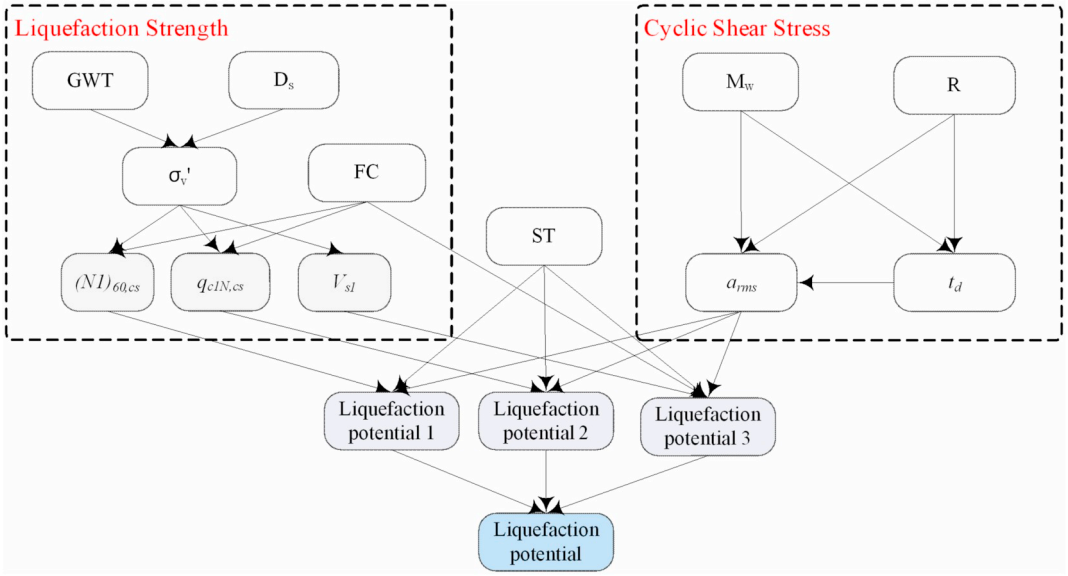

Fig. 5. A converging BN model for evaluating soil liquefaction based on multiple in-situ tests.

Table 4
Training and validating performances of the Converging BN model.

Dataset	*Macro-accuracy*	*Macro-AUC*	Liquefaction			Non-liquefaction		
			Macro-recall	*Macro-precision*	*Macro-F_1*	*Macro-recall*	*Macro-precision*	*Macro-F_1*
Training	0.949	0.990	0.985	0.947	0.966	0.845	0.957	0.897
Validating	0.890	0.966	0.968	0.896	0.929	0.673	0.893	0.753

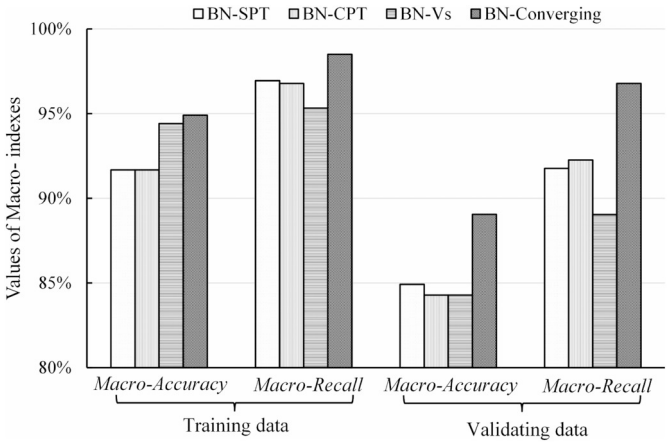

Fig. 6. Comparison of classification capacities of the four BN models.

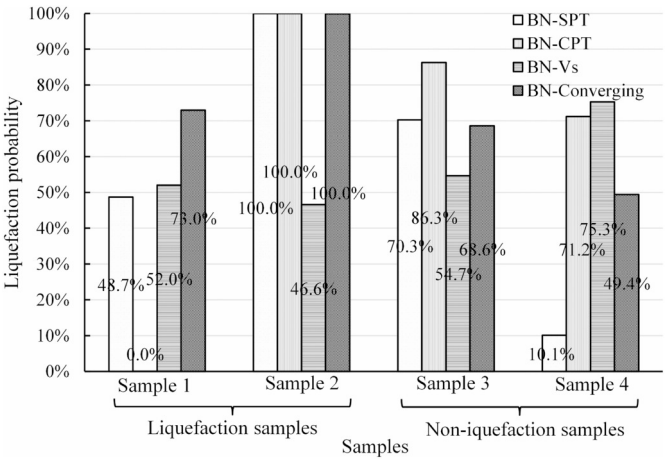

Fig. 7. Prediction probabilities of four samples in the four BN models.

$$P(LP=1 \mid LP1, LP2, LP3) = \frac{P(LP1, LP2, LP3 \mid LP=1)\cdot P(LP=1)}{P(LP1, LP2, LP3)} = \frac{\prod_{i=1}^{3} P(LP_i \mid LP=1)\cdot P(LP=1)}{\sum P(LP1)P(LP2)P(LP3)} \quad (7)$$

where LP1, LP2, and LP3 are marginally independent; P(LP = 1) is the prior probability; $\Sigma P(LP1)P(LP2)P(LP3)$ is the sum of the joint posterior probability given values of $(N1)_{60cs}$, q_{c1Ncs}, V_{s1}, soil type, and a_{rms}; P(LP_i) is the prediction value of one of the three BN models based on SPT, CPT, and V_s. Therefore, Eq. (7) unites the prediction probabilities of LP1, LP2, and LP3 to eliminate the contradiction between them.

The three in-situ tests have individual advantages, as mentioned in the Introduction section. Therefore, adopting two or more different in-situ test data simultaneously is beneficial for improving prediction accuracy and avoiding the phenomenon of paradox results. However, data for sites with three simultaneous in situ tests are scarce. However, there is a way to deal with the problem by studying the relationships among $(N1)_{60}$, q_{c1}, and V_s (Akca, 2003; McGann et al., 2017), which needs to further study.

5.3. Comparison of the BN models and other methods

Because of the various uncertainties of parameter or model, earthquake-induced liquefaction prediction is particularly suited to the probabilistic analysis. Several probabilistic models based on SPT, CPT, or V_s in this study are compared, in which the CPT-BI, V_s-AS, and CPT-YM models take an earthquake-induced liquefaction as a classification problem in a two-dimensional plane using CRR or measurements (e.g.,

q_{c1Ncs} in the CPT-YM model) versus CSR to find an optimal limit-state function, this kind of empirical simplification or dimensionality reduction will bring various uncertainties into the models.

However, the Bayesian updating framework (Moss et al., 2006; Kayen et al., 2013) and Bayesian Network (BN) models do not need to calculate the CRR, and they take on soil liquefaction as a high-order probabilistic problem associated with various input variables. The major advantage of three Bayesian approaches, the Bayesian updating framework, Bayes classifier based on the KDE and Bayesian Network (BN), is the facility to incorporate prior information and observed data. Even though these three methods all utilize the Bayesian theory, the Bayesian updating framework is a regression method, and it is difficult to find a suitable functional form. In the Bayes classifier method, the CSR needs to be calculated by the semi-empirical formula (see Eq. (A2)), which may bring various uncertainties of parameters and models into the classifier. In addition, the simplification into a two-dimensional classification problem, i.e. q_c versus CRR, may also lose part of the data information. In comparison the BN models in this study do not have any empirical formulas or parametric regressions among the input variables. In the proposed BN models in this study, the relationship between any two variables is presented by the conditional probability, and the indirect effects among the variables can be transmitted by the posterior probability. Another difference is that the proposed BN models do not need to calculate the CSR, which avoids the uncertainties. In addition, a new variable a_{rms} is considered in the proposed BN models that can consider the effect of amplitude, duration, and frequency on soil liquefaction.

The *Macro-F_1* values for the non-liquefaction samples in both training and prediction in this study are smaller than those for the liquefaction samples (as shown in Tables 2 and 3) due to the influence of the sampling bias (2.7:1 and 2.4:1 for liquefaction/non-liquefaction in the CPT and V_s datasets, respectively). The sampling bias ratios are larger than the recommended ranges in previous studies (Hu et al., 2017; Moss et al., 2006; Jain, 2012). However, the influence of sampling bias on prediction accuracy can be reduced by using oversampling or undersampling techniques (Hu et al., 2017). The *Macro-Accuracy* values of the BN-CPT and BN-V_s models are slightly improved to 0.878 and 0.890 in the prediction, respectively after using the oversampling technology. Also, the *Macro-F_1* values of the BN-CPT and BN-V_s models for the non-liquefaction samples are improved to 0.755 and 0.806, respectively.

6. Conclusions

In this study, the CPT and V_s databases from 25 historical earthquakes are first used to construct two new BN models considering the physical relation and conditional independence among the variables. These new models take the evaluation of earthquake-induced liquefaction as a classification problem in a high dimensional space without any empirical formulas or parametric regressions. The performance of the two BN models for evaluating soil liquefaction is compared with different liquefaction triggering analysis models. The findings show that the BN models are all more accurate than the simplified methods and the Bayes classifier based on the KDE method mentioned in this paper. In addition, a converging BN model is constructed combining the SPT, CPT and V_s databases to further improve its predictive ability and expand its applicability in different in-situ test conditions. More importantly, the converging BN model can avoid the paradox prediction results in the BN- SPT, CPT, and V_s models for the same case. After comparing the converging BN model with the two new BN models, it can be found that the converging BN model performs the best for evaluating soil liquefaction based on one of the in-situ testing data sets, but also multiple in-situ testing data sets, and the SPT-based BN model is the second best model. However, the V_s-based BN model is the worst model tested.

All of the BN models can accurately predict earthquake-induced liquefaction potential and diagnose liquefied or non-liquefied sites to detect what kind of conditions are likely to result in these situations, and they also can provide the graphical output for direct and visual use (see Appendix E). Since spatial variability of input variables such as a_{rms}, SPT number, cone tip resistance, and shear wave velocity might affect the prediction accuracy of the BN models, it requires to further study.

Notation

CPT	Cone penetration test
V_s	shear wave velocity
SPT	standard penetration test
CRR	cyclic resistance ratio
CSR	cyclic stress ratio
F_S	the factor of safety
MSF	magnitude scaling factor
K_σ	overburden correction factor
r_d	shear stress reduction factor
LP	liquefaction potential
P_L	probability of liquefaction
$(N1)_{60}$	normalized SPT blow count
$(N1)_{60cs}$	corrected SPT blow count for σ_v' and FC
FC	fines content
q_c	cone tip resistance
q_{c1}	normalized tip resistance
q_{c1Ncs}	a dimensionless quantity
p_a	one normal atmosphere
C_q	a correction factor
R_f	the friction ratio
V_{s1}	overburden stress-corrected shear wave velocity
V_{s1cs}	equivalent clean soil value of V_{s1}
$V_{s,\ 12m}{}^*$	average V_s in the upper 12.2 m of the soil column
K_{cs}	a correction factor
$\sigma_{\varepsilon r_d}$	the standard deviation of r_d
e	an exponential symbol
a_{rms}	root mean square of acceleration
PGA	peak ground acceleration
t_5	the moment at 5% of Arias intensity
t_{95}	the moment at 95% of Arias intensity
t_d	relative duration
M_w	earthquake magnitude
R	epicentral distance
ST	soil type
GWT	groundwater table
D_s	depth of soil deposit
σ_v'	vertical effective overburden stress
σ_V	vertical total overburden stresses
I_c	soil behavior type index
AUC	area under the curve
ROC	the receiver operating characteristic
B	*Brier score*
Φ	standard cumulative normal distribution

Acknowledgments

This work was supported by the National Natural Science Foundation of China, China (Grant No. 41702303). Part of the acceleration records from the 2003 Bachu earthquake and the 2008 Wenchuan earthquake used for this study were provided by the China Strong Motion Network Centre at the Institute of Engineering Mechanics, China Earthquake Administration; the authors thank the Institute for its support.

Appendix A. The Boulanger and Idriss model for the CPT database

The "simplified procedure" proposed by Seed and Idriss (1971) for predicting soil liquefaction triggering in terms of the factor of safety (F_S) defined as

$$F_S = {CRR}/{CSR} \tag{A1}$$

where CSR is the earthquake-induced cyclic stress ratio and SRR is the cyclic resistance ratio. When $F_S > 1.0$, the soil is not liquefied, and when $F_S < 1.0$, the soil is predicted to be liquefied.

Idriss and Boulanger (2006) improved CSR considering the magnitude scaling factor (MSF) and overburden correction factor (K_σ) for the reference values of $M_w = 7.5$ and $\sigma_{vs}' = 1\ atm$ (101.3 kPa); the re-evaluated CSR expression is:

$$CSR_{M_w=7.5,\sigma'_{vc}=1atm} = 0.65 r_d \frac{\sigma_V}{\sigma'_V}\frac{a_{\max}}{g}\frac{1}{MSF}\frac{1}{K_\sigma} \tag{A2}$$

where σ_V and σ_V' are the vertical total and effective overburden stresses, respectively; g is the acceleration of gravity; $a_{\max}$ is peak ground surface acceleration; r_d is shear stress reduction factor that can be calculated by

$$r_d = \exp[0.106M_w + 0.118M_w \sin(5.142 + (z/11.28)) - 1.012 - 1.126\sin(5.133 + (z/11.73))] \tag{A3}$$

where z is the depth of interest and M_w is the moment magnitude of the earthquake. The term MSF is computed as

$$MSF = 6.9\exp\left(-\frac{M_w}{4}\right) - 0.058 \le 1.8 \tag{A4}$$

Boulanger and Idriss, 2014 rewrote the MSF in a more general form as

$$MSF = 1 + (MSF_{\max} - 1)\left(8.64\exp\left(-\frac{M_w}{4}\right) - 1.325\right) \tag{A5}$$

where $MSF_{\max}$ is related to q_{c1Ncs} that can be calculated by

$$MSF_{\max} = 1.09 + \left(\frac{q_{c1NCS}}{180}\right)^3 \le 2.2 \tag{A6}$$

and the term $K_\sigma$is computed as:

$$K_\sigma = 1 - C_\sigma \ln\left(\frac{\sigma'_v}{P_a}\right) \le 1.1,\quad C_\sigma = \frac{1}{37.3 - 8.27(q_{c1Ncs})^{0.264}} \le 0.3 \tag{A7}$$

The CPT-based approach can be modified to account for the effects of fines content of soils on the liquefaction resistance that was proposed by Idriss and Boulanger (2008). The corrected equivalent clean sand q_{c1Ncs} value can be computed as

$$q_{c1Ncs} = q_{c1N} + \Delta q_{c1N} \tag{A8}$$

One of the first requirements would be to modify the cone bearing, q_c, to an overburden stress level of 100 kPa so that it is independent of σ_{v0}' and is more uniquely relate to the relative density of sandy soils. The normalization is taken as

$$q_{c1N} = C_q \frac{q_c}{P_a} \tag{A9}$$

where q_{c1N} is a dimensionless quantity, q_c is the cone tip resistance, p_a is one normal atmosphere that is approximately 101 kPa, and C_q is the correction factor that is similar to the correction coefficient C_N in the SPT procedure (Seed et al., 1985). Boulanger and Idriss, 2014 proposed an expression for C_q based on theoretical can experimental data that is expressed in the form

$$C_q = (P_a/\sigma'_{v0})^\beta \le 1.7,\quad \beta = 1.338 - 0.249(q_{c1Ncs})^{0.264} \tag{A10}$$

where the exponent β can be constrained to its recommend limits of 0.264–0.782 by limiting q_{c1Ncs} to between 21 and 254. The iterative computation of Eqs. (A9) and (A10) can be easily accomplished in Excel or other programming languages.

The resulting expression for Δq_{c1N} depends on both fines content and q_{c1N} that was updated by Boulanger and Idriss (2014), considering the effect of the new MSF and an increased weighting towards improving consistency with the empirical q_c/N_{60} ratios. The adjusted expression is as follows:

$$\Delta q_{c1N} = \left(11.9 + \frac{q_{c1N}}{14.6}\right)\cdot\exp\left[1.63 - \frac{9.7}{FC+2} - \left(\frac{15.7}{FC+2}\right)^2\right] \tag{A11}$$

where FC is percent fines content expressed as an integer.

The adjusted CRR for $M_w = 7.5$ and $\sigma_{vc}' = 1\ atm$ can be expressed as

$$CRR = \exp\left[\frac{q_{c1Ncs}}{113} + \left(\frac{q_{c1Ncs}}{1000}\right)^2 - \left(\frac{q_{c1Ncs}}{140}\right)^3 + \left(\frac{q_{c1Ncs}}{137}\right)^4 - 2.8\right] \tag{A12}$$

The recommended equation for the probability of liquefaction using the maximum likelihood method (Boulanger and Idriss (2014) is

$$P_L(q_{c1Ncs}, CSR_{M_w=7.5,\sigma'_{vc}=1atm}) = \Phi\left[-\frac{\frac{q_{c1Ncs}}{113} + \left(\frac{q_{c1Ncs}}{1000}\right)^2 - \left(\frac{q_{c1Ncs}}{140}\right)^3 + \left(\frac{q_{c1Ncs}}{137}\right)^4 - 2.6 - \ln(CSR_{M_w=7.5,\sigma'_{vc}=1atm})}{0.2}\right] \tag{A13}$$

where the value of P_L with 16% is the threshold for predicting soil liquefaction.

Appendix B. The Moss model for the CPT database

Moss et al. (2006) developed a robust and defensible probabilistic-based approach for assessing seismic soil liquefaction using the Bayesian updating method that allowed for treatment of parameter and model uncertainties. The expression of evaluation is as follows:

$$P_L(q_{c1}, R_f, CSR, M_w, \sigma'_V) = \Phi\left(-\frac{q_{c1}^{1.045} + q_{c1}(0.11R_f) + (0.11R_f) + c(1 + 0.85R_f) - 7.177\cdot \ln(CSR) - 0.848\ln(M_w) - 0.002\ln(\sigma'_V) - 20.923}{1.632}\right) \tag{B1}$$

where P_L is the probability of liquefaction, and the threshold for predicting soil liquefaction is approximately 15%; Φ is the standard cumulative normal distribution; R_f is the friction ratio that equals to the ratio of the sleeve to tip resistance. The expression of CSR can be calculated by:

$$CSR = 0.65 r_d \frac{\sigma_V}{\sigma'_V}\frac{a_{\max}}{g} \tag{B2}$$

where r_d can be evaluated for a given depth, peak ground acceleration, and moment magnitude. The expressions of r_d can be calculated using the following equations:

$$r_d(d, M_w, a_{\max}) = \begin{cases} \dfrac{1 + \frac{-9.147 - 4.173a_{\max} + 0.652M_w}{10.567 + 0.089e^{0.089(-3.28d - 7.76a_{\max} + 78.576)}}}{1 + \frac{-9.147 - 4.173a_{\max} + 0.652M_w}{10.567 + 0.089e^{0.089(-7.76a_{\max} + 78.576)}}} & for\ d < 20m \\ \dfrac{1 + \frac{-9.147 - 4.173a_{\max} + 0.652M_w}{10.567 + 0.089e^{0.089(-3.28d - 7.76a_{\max} + 78.576)}}}{1 + \frac{-9.147 - 4.173a_{\max} + 0.652M_w}{10.567 + 0.089e^{0.089(-7.76a_{\max} + 78.576)}}} - 0.0014(3.28d - 65) & for\ d \geq 20m \end{cases} \tag{B3}$$

where d is depth in meters at the midpoint of the critical layer.

q_{c1} is the normalized tip resistance that is as follows:

$$q_{c1} = \left(\frac{P_a}{\sigma'_v}\right)^c q_c \tag{B4}$$

$$c = 0.78(q_c)^{-0.33}\left(\frac{R_f}{|(\log(10 + q_c))^{1.21}|}\right)^{0.32(q_c)^{-0.35} - 0.49} \tag{B5}$$

Appendix C. The Andrus and Stokoe model for the V_s database

The equivalent CSR can be calculated with the following equation:

$$CSR_{M_w=7.5} = 0.65 r_d \frac{\sigma_V}{\sigma'_V}\frac{a_{\max}}{g}\frac{1}{MSF} \tag{C1}$$

where the expressions of r_d and MSF are given as follows:

$$r_d = \begin{cases} 1.0 - 0.00765z & for\ z \leq 9.15m \\ 1.174 - 0.0267z & for\ 9.15m < z \leq 23m \\ 0.744 - 0.008z & for\ 23m < z \leq 30m \end{cases} \tag{C2}$$

$$MSF = \left(\frac{M_w}{7.5}\right)^{-2.56} \tag{C3}$$

The overburden correction expression for V_s proposed by Robertson et al. (1992) was utilized as

$$V_{s1} = V_s\left(\frac{P_a}{\sigma'_{v0}}\right)^{0.25} \tag{C4}$$

where V_{s1} is the overburden stress-corrected shear wave velocity.

Considering the effect of fines content on V_{s1}, the clean soil equivalent can be expressed as (Robertson et al., 1992)

$$V_{s1cs} = K_{cs} V_{s1} \tag{C5}$$

where V_{s1cs} is the equivalent clean soil value of V_{s1} and K_{cs} is a correction of fines content to adjust the V_{s1} value to a clean soil equivalent. K_{cs} can be approximated using the following expression:

$$K_{cs} = \begin{cases} 1 & for\ FC \leq 5\% \\ 1 + (FC - 5)T & for\ 5\% < FC < 35\% \\ 1 + 30T & for\ FC \geq 35\% \end{cases} \tag{C6}$$

where

$$T = 0.009 - 0.0109\left(\frac{V_{s1}}{100}\right) + 0.0038\left(\frac{V_{s1}}{100}\right)^2 \tag{C7}$$

The CRR model proposed by Andrus and Stokoe II (2000) can be rewritten as

$$CRR = 0.022\left(V_{s1cs}/100\right)^2 + 2.8\left[1/(215 - V_{s1cs}) - \left(1/215\right)\right] \tag{C8}$$

where the constant 210 m/s is limiting V_{s1}, as recommended by Andrus and Stokoe II (2000). Juang et al. (2002) estimated the value of P_L from the probability density functions of F_s using Bayesian mapping function approach for probabilistic predicting soil liquefaction, and the relationship between P_L and F_s can be calculated by

$$P_L(F_S) = \frac{1}{1 + \left(F_S/0.73\right)^{3.4}} \tag{C9}$$

where the value of P_L with 0.26 is the threshold for predicting soil liquefaction.

Appendix D. The Kayen et al. model for the V_s database

Kayen et al. (2013) developed probabilistic correlations for seismic soil liquefaction occurrence based on V_s site data using a Bayesian regression and structural reliability methods. They argued that there is little difference between the V_s of sand and silty or clayey sand; thus, V_s measurements may be relatively insensitive to fines content. Therefore, there is a small positive influence of fines content on liquefaction resistance for the V_s-based procedure. The overburden stress-corrected shear wave velocity V_{s1} can refer to Eq. (C4), and the calculation of CSR can refer to Eq. (B2) in Appendix B, whereas r_d can be estimated by

$$r_d(d, a_{\max}, M_w, V^*_{s,12m}) = \frac{1 + \frac{-23.013 - 2.949a_{\max} + 0.999M_w + 0.0525V^*_{s,12m}}{16.258 + 0.201e^{0.341(-d + 0.0785V^*_{s,12m} + 7.586)}}}{1 + \frac{-23.013 - 2.949a_{\max} + 0.999M_w + 0.0525V^*_{s,12m}}{16.258 + 0.201e^{0.341(0.0785V^*_{s,12m} + 7.586)}}} \pm \sigma_{\varepsilon rd} \tag{D1}$$

where d is depth in meters, measured at the midpoint of the critical layer; $V_{s,\ 12m}{}^*$ is the average V_s in the upper 12.2 m of the soil column that expresses site stiffness, whereas if estimation of $V_{s,\ 12m}{}^*$ is considered difficult for a given case, its value can simply be taken as approximately 150–200 m/s for most potentially liquefied sites; and e is an exponential symbol. Additionally, $\sigma_{\varepsilon r_d}$ is the standard deviation of r_d, which can be calculated by

$$\begin{cases} \sigma_{\varepsilon r_d}(d) = 0.0198d^{0.85} & for\ d < 12.2m \\ \sigma_{\varepsilon r_d}(d) = 0.0198 \cdot 12.2^{0.85} & for\ d \geq 12.2m \end{cases} \tag{D2}$$

The expression of the probability of liquefaction (PL) terms as

$$P_L = \Phi\left(-\frac{(0.0073V_{s1})^{2.8011} - 1.946\ln(CSR) - 2.6168\ln(M_w) - 0.0099\ln(\sigma'_V) + 0.0028FC}{0.4809}\right) \tag{D3}$$

where the value of P_L with 0.15 is the threshold for predicting soil liquefaction.

Appendix E. Supplementary data

Supplementary data to this article can be found online at https://doi.org/10.1016/j.enggeo.2019.04.003.

References

Akca, N., 2003. Correlation of SPT-CPT data from the United Arab Emirates. Eng. Geol. 67 (3–4), 219–231.

Andrus, R.D., Stokoe II, K.H., 1997. Liquefaction resistance based on shear wave velocity. Proc., NCEER Workshop on Evaluation of Liquefaction Resistance of Soils. Nat. Ctr. for Earthquake Engrg. Res., State Univ. of New York at Buffalo 89–128.

Andrus, R.D., Stokoe II, K.H., 2000. Liquefaction resistance of soils from shear-wave velocity. J. Geotech. Geoenviron. 126 (11), 1015–1025 ASCE.

Bayraktarli, Y.Y., 2006. Application of Bayesian probabilistic networks for liquefaction of soil. In: 6th international Ph.D. symposium in civil engineering. 8. pp. 23–26 Zurich.

Bensi, M.T., Kiureghian, A.D., Straub, D., 2011. A Bayesian Network Methodology for Infrastructure Seismic Risk Assessment and Decision Support. Report No. 2011/02. Pacific Earthquake Engineering Research Centre, Berkeley.

Boulanger, R.W., Idriss, I.M., 2014. CPT and SPT Based Liquefaction Triggering Procedures. Report UCD/CGM-14/01. Davis, CA: Department of Civil and Environmental Engineering. University of California.

Brier, G.W., 1950. Verification of forecasts expressed in terms of probability. Mon. Weather Rev. 78 (1), 1–3.

Cao, Z.Z., 2010. Characteristics of soil liquefaction in the great Wenchuan Earthquake and procedures for gravelly soil liquefaction evaluation. Ph.D. dissertation. Institute of Engineering Mechanics, China Earthquake Administration, Harbin, China In Chinese.

Cao, Z.J., Zheng, S., Li, D., et al., 2018. Bayesian identification of soil stratigraphy based on soil behaviour type index. Can. Geotech. J. https://doi.org/10.1139/cgj-2017-0714.

Cetin, K.O., 2000. SPT-Based Probabilistic Assessment of Seismic Soil Liquefaction Initiation Hazard. Ph.D. dissertation. Univ. of California Berkeley. Calif.

Ching, J., Wang, J.S., Juang, C.H., et al., 2015. Cone penetration test (CPT)-based stratigraphic profiling using the wavelet transform modulus maxima method. Can. Geotech. J. 52 (12), 1993–2007.

Dong, L., 2010. Primary study on liquefaction in Bachu-Jiashi Earthquake. Master dissertation. Institute of Engineering Mechanics, China Earthquake Administration, Harbin, China In Chinese.

Friedman, N., Goldszmidt, M., 1996. Discretization of continuous attributes while learning Bayesian networks. In: Proceedings of the 13th International Conference on Machine Learning (ICML). Morgan Kaufmann Publishers, San Francisco, CA, pp. 157–165.

Friedman, N., Goldszmidt, M., Wyner, A., 1999. Data analysis with Bayesian networks: A bootstrap approach. In: Proceedings of the 15th Conference on Uncertainty in Artificial Intelligence. Morgan Kaufmann, Stockholm, Sweden, pp. 196–205.

Green Russell, A., Sneha, Upadhyaya, Wood Clinton, M., et al., 2017. Relative efficacy of CPT- versus V_s-based simplified liquefaction evaluation procedures. In: Proceedings of the 19th International Conference on Soil Mechanics and Geotechnical Engineering, pp. 1521–1524 Seoul, September.

Hu, Jilei, Liu, Huabei, 2019. Identification of ground motion intensity measure and its application for predicting soil liquefaction potential based on Bayesian network method. Eng. Geol. 248, 34–49.

Hu, J.L., Tang, X.W., Qiu, J.N., 2015. A Bayesian network approach for predicting seismic liquefaction based on interpretive structural modeling. Georisk: Assess. Manag. Risk Eng. Syst. Geohazards 9 (3), 200–217.

Hu, J.L., Tang, X.W., Qiu, J.N., 2016. Assessment of Seismic liquefaction potential based on Bayesian network constructed from domain knowledge and history data. Soil Dyn. Earthquake Eng. 89, 49–60.

Hu, J.L., Tang, X.W., Qiu, J.N., 2017. Analysis of the influences of sampling bias and class imbalance on performances of Probabilistic liquefaction models. Int. J. Geomech. 17 (6), 04016134.

Idriss, I.M., Boulanger, R.W., 2006. Semi-empirical procedures for evaluating liquefaction potential during earthquakes. Soil Dyn. Earthq. Eng. 26 (2–4), 115–130.

Idriss, I.M., Boulanger, R.W., 2008. Soil liquefaction during earthquakes. Monograph

MNO-12. Earthquake Engineering Research Institute, Oakland, CA.
Idriss, I.M., Boulanger, R.W., 2010. SPT-based liquefaction triggering procedures. In: Report No. UCD/CGM-10/02, Center for geotechnical modeling, Department of civil and environmental engineering, University of California at Davis.
Jain, A., 2012. Sampling bias in evaluating the probability of seismically induced soil liquefaction with SPT & CPT case histories. Masters Dissertation. Michigan Technological Univ., Houghton, MI.
Jensen, V.F., 1999. Gradient descent training of Bayesian networks. In: Proceedings of the European Conference on Symbolic and Quantitative Approaches to Reasoning and Uncertainty, pp. 190–200 (July 05-09).
Juang, C.H., Jiang, T., Andrus, R.D., 2002. Assessing probability-based methods for liquefaction potential evaluations. J. Geotech. Geoenviron. 128 (7), 580–589.
Juang, C.H., Ye, Fang Sunny, Hui, Khor Eng, 2006. First-order reliability method for probabilistic liquefaction triggering analysis using CPT. J. Geotech. Geoenviron. 132 (3), 337–350.
Juang, C.H., Lu, C.C., Hwang, J.H., 2009. Assessing probability of surface manifestation of liquefaction in a given exposure time using CPTU. Eng. Geol. 104, 223–231.
Juang, C.H., Ching, J.Y., Luo, Z., et al., 2012. New models for probability of liquefaction using standard penetration tests based on updated database of case histories. Eng. Geol. 133-134, 85–93.
Kayen, R., Moss, R.E.S., Thompson, E.M., et al., 2013. Shear-wave velocity-based probabilistic and deterministic assessment of seismic soil liquefaction potential. J. Geotech. Geoenviron. 139 (3), 407–419.
Kontkanen, P., Myllymaki, P., Silander, T., et al., 1997. Comparing predictive inference methods for discrete domains. In: Proceedings of the Sixth International Workshop on Artificial Intelligent and Statistics, Ft. Lauderdale, USA, pp. 311–318.
Ku, Chih-Sheng, Lee, Der-Her, Wu, Jian-Hong, 2004. Evaluation of soil liquefaction in the Chi-Chi, Taiwan earthquake using CPT. Soil Dyn. Earthq. Eng. 24 (9–10), 659–673.
Lauritzen, S.L., 1995. The EM algorithm for graphical association models with missing data. Comput. Stat. Data Anal. 19 (2), 191–201.
Maurer, B.W., Green, R.A., Cubrinovski, M., et al., 2015. Assessment of CPT-based methods for liquefaction evaluation in a liquefaction potential index (LPI) framework. Geotechnique 65 (5), 328–336.
McGann, C.R., Bradley, B.A., Cubrinovski, M., 2017. Development of a regional V_{s30} model and typical V_s profiles for Christchurch, New Zealand from CPT data and region-specific CPT-V_s correlation. Soil Dyn. Earthquake Eng. 95, 48–60.
Moss, R.E.S., Seed, R.B., Kayen, R.E., et al., 2006. CPT-based probabilistic and deterministic assessment of in situ seismic soil liquefaction potential. J. Geotech. Geoenviron. Eng. 132 (8), 1032–1051.
Olsen, R.S., Koester, J.P., 1995. Prediction of liquefaction resistance using the CPT. In: Proceedings of the International Symposium on Cone Penetration Testing, CPT'95, Linkoping, Sweden. vol. 2. SGS. Oct, pp. 251–256.
Oommen, T., Baise, L.G., Vogel, R., 2010. Validation and application of empirical liquefaction models. J. Geotech. Geoenviron. 136, 1618–1633.
Pearl, J., 1988. Probabilistic Reasoning in Intelligent Systems, Networks of Plausible Inference. Morgan Kaufmann, San Francisco, CA.
Robertson, P.K., Wride, C.E., 1998. Evaluation of cyclic liquefaction potential using the cone penetration test. Can. Geotech. J. 35 (3), 442–459.
Robertson, P.K., Campanella, R.G., Wightman, A., 1983. SPT-CPT correlations. J. Geotech. Eng. 109 (11), 1449–1459.
Robertson, P.K., Woeller, D.J., Finn, W.D.L., 1992. Seismic cone penetration test for evaluating liquefaction potential under cyclic loading. Can. Geotech. J. 29, 686–695.
Schneider, J.A., Moss, R.E.S., 2011. Linking cyclic stress and cyclic strain based methods for assessment of cyclic liquefaction triggering in sands. Geotech. Lett. 1, 31–36.
Seed, H.B., Idriss, I.M., 1971. Simplified procedure for evaluating soil liquefaction potential. J. Soil Mech. Found. Eng. Div., ASCE 97 (9), 1249–1273.
Seed, H.B., Idriss, I.M., 1982. Ground Motions and Soil Liquefaction during Earthquakes. Earthquake Engineering Research Institute Monograph. Oakland, CA.
Seed, H.B., Tokimatsu, K., Harder, L.F., Chung, R.M., 1985. The influence of SPT procedures in soil liquefaction resistance evaluations. J. Geotech. Geoenviron. 111 (12), 1425–1445 ASCE.
Seed, R.B., Cetin, K.O., Moss, R.E.S., et al., 2003. Recent advances in soil liquefaction engineering: A unified and consistent framework. In: Keynote Presentation, 26th Annual ASCE Los Angeles Geotechnical Spring Seminar, Long Beach, California, April 30.
Shen, M., Chen, Q., Zhang, J., et al., 2016. Predicting liquefaction probability based on shear wave velocity: an update. Bull. Eng. Geol. Environ. 75 (3), 1199–1214.
Tang, X.W., Bai, X., Hu, J.L., Qiu, J.N., 2018. Assessment of liquefaction-induced hazards using Bayesian networks based on standard penetration test data. Nat. Hazards Earth Syst. Sci. 18, 1451–1468.
Thevanayagam, S., 1998. Effect of fines and confining stress on undrained shear strength of silty sands. J. Geotech. Geoenviron. Eng. 124 (6), 479–491 ASCE.
Thompson, E.M., Baise, L.G., Kayen, R.E., 2007. Spatial correlation of shear-wave velocity in the San Francisco Bay Area sediments. Soil Dyn. Earthq. Eng. 27 (2), 144–152.
Wang, H., Wang, X., Wellmann, F., et al., 2018. A Bayesian unsupervised learning approach for identifying soil stratification using cone penetration data. Can. Geotech. J. https://doi.org/10.1139/cgj-2017-0709.
Wang, X., Wang, H., Liang, R.Y., et al., 2019. A semi-supervised clustering-based approach for stratification identification using borehole and cone penetration test data. Eng. Geol. 248, 102–116.
Wood, C.M., Cox, B.R., Green, R.A., et al., 2017. V_s-based evaluation of select liquefaction case histories from the 2010-2011 Canterbury Earthquake Sequence. J. Geotech. Geoenviron. Eng. ASCE 143 (9), 04017066.
Yang, Y., Chen, L.W., Sun, R., et al., 2017. A depth-consistent SPT-based empirical equation for evaluating sand liquefaction. Eng. Geol. 221, 41–49.
Yazdi, J.S., Moss, R.E.S., 2017. Nonparametric liquefaction triggering and postliquefaction deformations. J. Geotech. Geoenviron. Eng. 143 (3), 04016105.
Youd, T.L., Idriss, I.M., Andrus, R.D., et al., 2001. Liquefaction resistance of soils: summary report from the 1996 NCEER and 1998 NCEER/NSF workshops on evaluation of liquefaction resistance of soils. J. Geotech. Geoenviron. 127 (4), 817–833.